ENSO-Like and ENSO-Induced Tropical Pacific Decadal Variability in CGCMs

JUNG CHOI AND SOON-IL AN

Department of Atmospheric Sciences, Yonsei University, Seoul, South Korea

SANG-WOOK YEH

Department of Environmental Marine Science, Hanyang University, Ansan, South Korea

JIN-YI YU

Department of Earth System Science, University of California, Irvine, Irvine, California

(Manuscript received 19 February 2012, in final form 26 July 2012)

ABSTRACT

Outputs from coupled general circulation models (CGCMs) are used in examining tropical Pacific decadal variability (TPDV) and their relationships with El Niño–Southern Oscillation (ENSO). Herein TPDV is classified as either ENSO-induced TPDV (EIT) or ENSO-like TPDV (ELT), based on their correlations with a decadal modulation index of ENSO amplitude and spatial pattern. EIT is identified by the leading EOF mode of the low-pass filtered equatorial subsurface temperature anomalies and is highly correlated with the decadal ENSO modulation index. This mode is characterized by an east–west dipole structure along the equator. ELT is usually defined by the first EOF mode of subsurface temperature, of which the spatial structure is similar to ENSO. Generally, this mode is insignificantly correlated with the decadal modulation of ENSO. EIT closely interacts with the residuals induced by ENSO asymmetries, both of which show similar spatial structures. On the other hand, ELT is controlled by slowly varying ocean adjustments analogous to a recharge oscillator of ENSO. Both types of TPDV have similar spectral peaks on a decadal-to-interdecadal time scale. Interestingly, the variances of both types of TPDV depend on the strength of connection between El Niño–La Niña residuals and EIT, such that the strong two-way feedback between them enhances EIT and reduces ELT. The strength of the two-way feedback is also related to ENSO variability. The flavors of El Niño–La Niña with respect to changes in the tropical Pacific mean state tend to be well simulated when ENSO variability is larger in CGCMs. As a result, stronger ENSO variability leads to intensified interactive feedback between ENSO residuals and enhanced EIT in CGCMs.

1. Introduction

Tropical Pacific decadal variability (TPDV) is an important component of global-scale climate variability (Mantua et al. 1997; Zhang et al. 1997), which is known to be related to the Pacific–North America pattern (Wallace and Gutzler 1981) in the Northern Hemisphere as well as the atmospheric circulation near the Southern Ocean and Antarctica (Garreaud and Battisti 1999). The dominant mode of TPDV is characterized by broad triangular-shaped sea surface temperature (SST) variations exhibiting a warmer than normal tropical central-to-eastern Pacific and a colder than normal extratropical central North Pacific or vice versa (Latif et al. 1997). The SST variations associated with TPDV have been detected in observations (Evans et al. 2002). In the mid-1970s, a distinctive triangular-shaped SST warming anomaly pattern existed in the tropical eastern Pacific (Zhang et al. 1997; Luo and Yamagata 2001; Ashok et al. 2007). This decadal variability shows a structure largely similar to El Niño–Southern Oscillation (ENSO) in the tropical Pacific, yet this type of structure is typically more prominent over the extratropical North Pacific (Zhang et al. 1997). Many previous studies (Knutson and Manabe 1998; Luo et al. 2003; Wang et al. 2003) have documented

Corresponding author address: Prof. Soon-Il An, Department of Atmospheric Sciences, Yonsei University, Seoul 120-749, South Korea.
E-mail: sian@yonsei.ac.kr

DOI: 10.1175/JCLI-D-12-00118.1

that a slow ocean adjustment process on a decadal-to-interdecadal time scale accounts for phase transition analogous to the recharge/discharge oscillator of ENSO (Jin 1997a,b). Therefore, this TPDV is usually known as ''ENSO-like tropical Pacific decadal variability.'' This is the most dominant mode of equatorial Pacific temperature variation on a decadal-to-interdecadal time scale.

Meanwhile, ENSO properties, including amplitude, frequency, and spatial distribution, vary on a decadal-to-interdecadal time scale (An 2004, 2009; Sun and Yu 2009; Choi et al. 2011). This decadal modulation of ENSO properties has been explained by several different theories. On the one hand, some studies (Zebiak 1989; Jin et al. 1994; Timmermann 2003) have emphasized the nonlinear internal dynamics of the coupled tropical system as the basis for the modulation, and others (Kirtman and Schopf 1998; Flügel and Chang 1999; Burgman et al. 2008) have proposed the importance of stochastic forcing generated by the atmospheric noise. On the other hand, other studies have pointed out that changes in the tropical Pacific mean state could lead to changes in ENSO properties (An and Wang 2000; Fedorov and Philander 2000; An et al. 2006; Dewitte et al. 2007; Bejarano and Jin 2008). In other words, the change in mean state associated with TPDV appears to be a plausible reason for decadal ENSO modulation (Choi et al. 2009; Li et al. 2011; Yu and Kim 2011). However, another study demonstrated that there is little or no relationship between the ENSO-like TPDV and decadal modulation of ENSO in CGCM (Yeh and Kirtman 2004). Instead, the second mode of TPDV is more closely related to decadal ENSO modulation. The spatial pattern of the second empirical orthogonal function (EOF) mode is quite different from the ENSO-like TPDV pattern. Timmermann (2003) has also pointed out that the second EOF mode, which reflects subsurface temperature anomalies in the equatorial Pacific that exhibit an east–west dipole-like structure, are strongly related to decadal ENSO modulation. Furthermore, Sun and Yu (2009) demonstrated that observed TPDV with a notable east–west dipole-like spatial structure could be induced by the rectification effect of ENSO. Also, Dewitte et al. (2009) studied the relationship between the first two EOF modes of low-frequency subsurface temperature and the ENSO modulation from the SODA reanalysis data. In this regard, the decadal modulation of ENSO does not appear to be related to the ENSO-like mode but rather the dipole-like mode of TPDV.

The origin of the dipole-like mode of TPDV is suggested to be the statistical residual for asymmetric anomaly patterns associated with El Niño and La Niña events (Rodgers et al. 2004; Cibot et al. 2005; Schopf and Burgman 2006; Sun and Yu 2009). Those studies demonstrated that the residuals, owing to asymmetries between El Niño and La Niña in their spatial patterns and amplitudes, could rectify into a background condition and lead a slowly varying variability. Using high-quality and in situ ocean datasets, McPhaden et al. (2011) recently argued that decadal change in the tropical Pacific SST during the 2000s, resembling a dipole-like structure, is due to a greater occurrence of central Pacific warming events—for example, central Pacific El Niño (Yu and Kao 2007; Kao and Yu 2009; Yeh et al. 2009), warm pool El Niño (Kug et al. 2009), and El Niño Modoki (Ashok et al. 2007)—but not the other way around. Likewise, Choi et al. (2012) argued that the statistical residuals as a result of El Niño–La Niña asymmetry representing an east–west dipole structure could feed into the tropical Pacific mean state. Interestingly, both the residual pattern due to ENSO asymmetry and the mean state pattern correlated to the decadal modulation of ENSO show similar east–west dipole-like structures, suggesting a strong dynamic relationship between them that is worthy of further investigation.

According to these previous studies, at least two types of TPDVs exist. One is ENSO-like TPDV, which has a spatial structure resembling ENSO (i.e., triangular structure in SST anomaly; referred to as ENSO-like TPDV). The other type is related to decadal ENSO modulation, which has an east–west dipole structure in the tropical Pacific (referred to as ENSO-induced TPDV). Several studies demonstrating the relationship between these two types of TPDVs have been conducted. Yeh and Kirtman (2004) demonstrated that ENSO-like TPDV accounts for a larger percentage variance of decadal SST variability than does ENSO-induced TPDV in a coupled general circulation model (CGCM). They also showed that the variance of ENSO-like TPDV grew larger as the amplitude of atmospheric noise increased. Choi et al. (2012) demonstrated that ENSO-induced TPDV somehow experienced a phase transition of ENSO-like TPDV. That study's results imply that these two types of TPDVs are linearly independent but related. Nevertheless, their relationship is not yet fully understood. Furthermore, it is unclear why different CGCMs produce different relative strengths of these two TPDV types (e.g., Yu and Kim 2011).

Overall, the primary interest of this study is to examine the relationship between ENSO-like and ENSO-induced TPDVs in CGCMs. Furthermore, the associations between both TPDV modes and the simulated ENSO will be investigated. Section 2 describes the datasets and CGCMs used in this study. Section 3 describes the

TABLE 1. Model descriptions. Niño-3.4 STD indicates the standard deviation of the SST anomaly averaged over the Niño-3.4 region (5°S–5°N, 170°–120°W).

No.	Models	Institution	Integration period (yr)	Niño-3.4 STD
0	SODA 2.2.4 (Reanalysis)	Texas A&M (TAMU)/University of Maryland (UMD), USA	138	0.744
1	CCCMA T47	Canadian Centre for Climate Modelling and Analysis (CCCma), Canada	500	0.458
2	CCCMA T63	CCCma, Canada	400	0.468
3	CCSM 3.0	National Center for Atmospheric Research (NCAR), USA	300	0.868
4	CNRM CM3	Centre National de Recherches Météorologiques (CNRM), France	500	1.610
5	GFDL CM2.0	National Oceanic and Atmospheric Administration (NOAA) Geophysical Fluid Dynamics Laboratory (GFDL), USA	500	0.977
6	GFDL CM2.1	NOAA GFDL, USA	500	1.300
7	GISS EH	National Aeronautics and Space Administration (NASA)/Goddard Institute for Space Studies (GISS), USA	400	0.750
8	GISS ER	NASA/GISS, USA	500	0.214
9	INM CM3	Institute of Numerical Mathematics (INM), Russia	330	0.979
10	IPSL CM4	L'Institut Pierre-Simon Laplace (IPSL), France	500	0.994
11	MIROC 3.2 medres	Center for Climate System Research (CCSR), Japan	500	0.499
12	MIUB ECHOG	Meteorological Institute of the University of Bonn (MIUB), Germany	341	1.398
13	MRI 2.3	Meteorological Research Institute (MRI), Japan	350	0.780
14	UKMO HadCM3	Met Office, UK	341	0.907

classification of the two TPDVs in the CGCMs and their spatial characteristics. Section 4 shares details on the relationship between the two TPDVs and ENSO, and section 5 provides a summary and discussion of the study.

2. Data

General information about the CGCMs used in this study is summarized in Table 1, which consists of 14 models from phase 3 of the Coupled Model Intercomparison Project (CMIP3; Meehl et al. 2007) CGCMs. All models selected for this study were integrated for more than 300 years using preindustrial CO_2 levels at 280 ppmv. To check the model's performance in the tropical Pacific climate, we compared the climatological vertical gradient of subsurface temperatures along the equatorial Pacific (5°S–5°N). The Simple Ocean Data Assimilation (SODA) reanalysis set (Carton et al. 2005; Carton and Giese 2008) was mapped onto a uniform $0.5° \times 0.5°$ grid, and the most recent version (SODA 2.2.4) including monthly averages from 1871 to 2008 was analyzed in this study.

Figure 1 includes the longitude–depth cross section describing the climatology of the vertical temperature gradient along the equatorial Pacific (5°S–5°N). The vertical axis represents the depth (in meters). The vertical gradient of temperature is used to measure subsurface ocean stratification and to determine the depth of the thermocline, both of which are important factors in ocean dynamics (Sverdrup et al. 1942). Additionally, the strength of stratification near the thermocline plays a crucial role in ENSO dynamics (Timmermann et al. 1999; Fedorov and Philander 2000, 2001; Thual et al. 2011). The simulated structure of the vertical temperature gradient is one key factor in understanding the performance of ENSO simulation in CGCMs. In Fig. 1a, the SODA has a maximum gradient of 0.15 K m^{-1} near 160° and 90°W. The maximum gradient gets shallower toward to the eastern Pacific. This indicates a shoal thermocline depth over the eastern tropical Pacific due to the trade winds, which is an important factor for ENSO (Collins et al. 2010). The shoaling thermocline structure is missing in three CGCMs: CCCMA T47, CCCMA T63, and GISS ER. Additionally, INM CM3 and MIROC3.2(medres) show excessively weak stratifications in the central tropical Pacific. According to Yu and Kim (2011), there is an insignificant correlation between the decadal ENSO modulation index and the principal component time series of the leading EOFs from TPDV in two CGCMs: GISS EH and UKMO HadCM3 (Fig. 4 in Yu and Kim 2011). In CNRM CM3, the spatial pattern of TPDV association in the decadal ENSO modulation represented a weak east–west dipole-like structure unlike those of the other CGCMs (Fig. 3 in Yu and Kim 2011). After considering the performance of simulated ENSO and tropical Pacific decadal variability, we selected six CGCMs for further analysis: CCSM3.0, GFDL CM2.0, GFDL CM2.1, IPSL CM4,

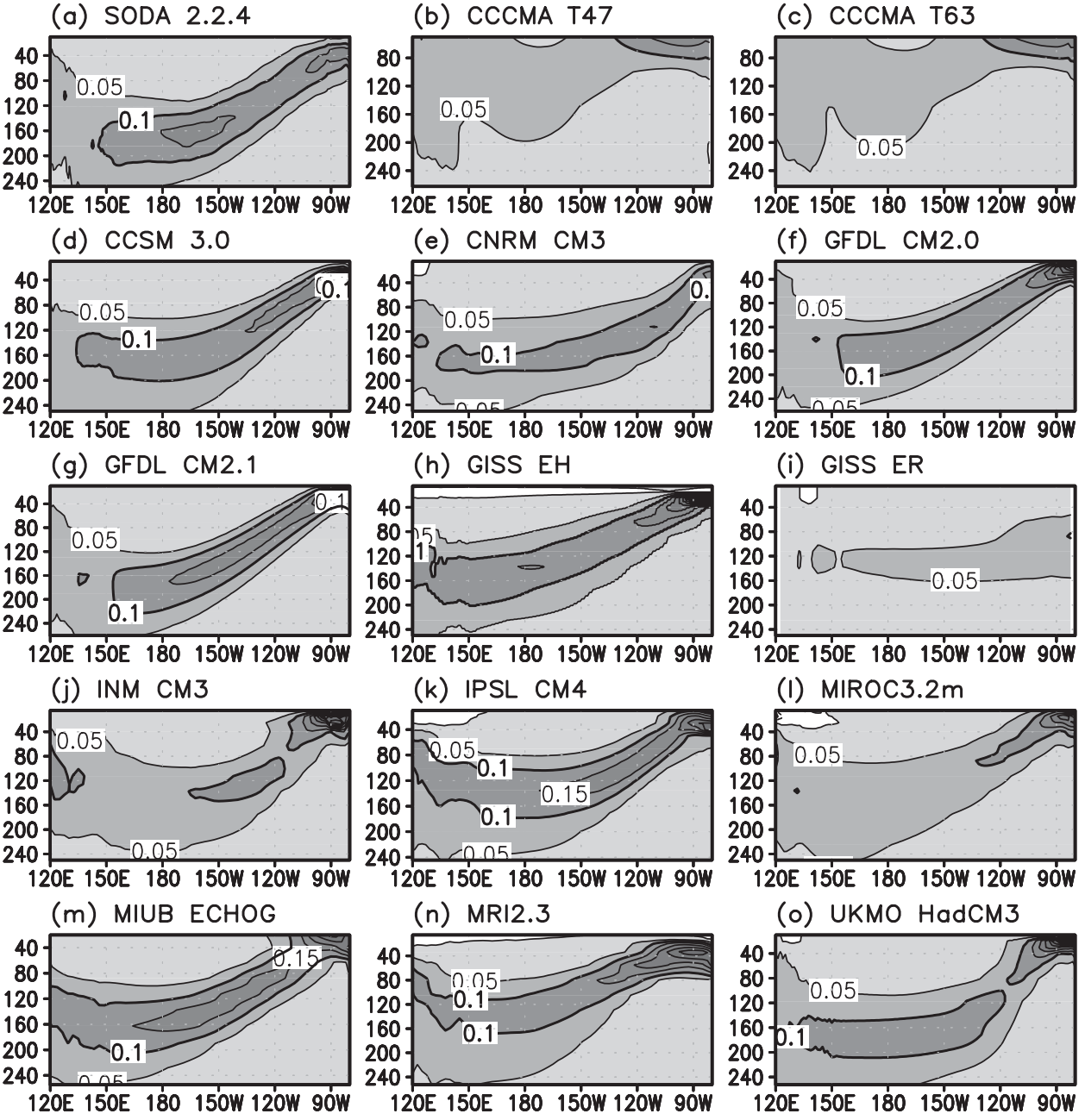

FIG. 1. Longitude–depth cross section of the climatology of the vertical temperature gradient (5°S–5°N).

MIUB ECHOG, and MRI 2.3. The selected CGCMs will be analyzed in the next several sections based on the relationship between ENSO and tropical Pacific decadal variability and the possible mechanisms.

3. Two modes of TPDVs in CGCMs

To identify TPDVs in the CGCMs, we performed an empirical orthogonal function analysis (also known as principal component analysis) of equatorial (5°S–5°N) subsurface temperature anomalies from the surface to a 250-m depth. Previous studies used SST anomalies to identify ENSO or TPDV (Yu and Boer 2004; Imada and Kimoto 2009; Yu and Kim 2011). In this study, we used averaged subsurface temperature anomalies of the equator, as suggested in Choi et al. (2011, 2012), to identify subsurface ocean structures that store long-term memory for climate variability. The anomalies were

TABLE 2. The first column refers to CGCM names. The second and third columns indicate the ENSO-induced TPDV and the temporal correlation between its PC time series and decadal ENSO modulation index (10-yr sliding standard deviation of Niño-3.4 SSTA). The third and fourth columns indicate the ENSO-like TPDV and the temporal correlation between its PC time series and decadal ENSO modulation index.

	Models	ENSO-induced TPDV (variance, %)	Temporal correlation	ENSO-like TPDV (variance, %)	Temporal correlation
1	CCSM 3.0	EOF2 (23.28)	0.69*	EOF1 (39.19)	0.03
2	GFDL CM2.0	EOF3 (19.48)	0.84*	EOF1 (33.59) EOF1 + 2 (59.67)	0.19
3	GFDL CM2.1	EOF1 (59.13)	0.91*	EOF2 (21.51)	0.23
4	IPSL CM4	EOF2 (23.50)	0.79*	EOF1 (43.20)	0.24
5	MIUB ECHOG	EOF1 (53.43)	0.91*	EOF2 (19.57)	0.20
6	MRI2.3	EOF2 (27.39)	0.56*	EOF1 (39.17)	0.27

* Statistically significant at 99% confidence level.

detected by removing seasonal climatology. The first columns in Fig. 2 show the spatial patterns of the first leading EOF modes from the six selected CGCMs. These leading modes have a spectral peak near the interannual band (not shown), which is related to the ENSO time scale. In the first columns of Fig. 3, regressions of tropical Pacific SST anomalies associated with the principal components of these leading EOF modes further confirm that the leading modes of Fig. 2 are the simulated ENSO in the CGCMs. Figure 3 demonstrates that the SST anomaly center of the simulated ENSO tends to be located more westward compared to the observations, which is a model deficiency common to many CGCMs due to a strong simulated cold tongue (Latif et al. 2001; AchutaRao and Sperber 2002; Hannachi et al. 2003). Nevertheless, the general features of the simulated ENSO are reasonably realistic compared with observations that indicate a large positive anomaly over the equatorial region and a weak negative anomaly over the western off-equatorial region. The ENSO simulated in GFDL CM2.1 and MIUB ECHOG is stronger than that of other models. The structures shown in the first columns of Fig. 2 represent the subsurface ocean structure during the peak phase of El Niño events. There is basin-scale warming at the surface and a dipole structure along the thermocline depth. These features are consistent with the conventional characteristics of El Niño, including a deeper mean thermocline depth and accumulated heat content over the eastern tropical Pacific (Jin 1997a,b).

A 10-yr sliding average was applied to the ocean temperature anomalies to obtain decadal variability. An EOF analysis was then applied to the decadal anomalies to obtain leading modes of TPDV. To identify the ENSO-induced mode of TPDV, we defined a decadal modulation index of ENSO amplitude, which is calculated as the 10-yr sliding standard deviation for the Niño-3.4 (averaged over 5°S–5°N, 170°–120°W) SST anomalies. We then calculated the temporal correlation between the decadal modulation index of ENSO and the principal component (PC) time series of the leading decadal modes of TPDV. The EOF mode with the highest temporal correlation was classified as the ENSO-induced TPDV. The second column in Fig. 2 displays the ENSO-induced TPDV from the six selected CGCMs. As demonstrated in the figures, the longitude–depth structure of ENSO-induced TPDV is characterized by an east–west dipole structure. This feature is generally simulated by the six CGCMs, with the exception of CCSM3.0, which has a weak warming on the eastern side. The percentage of variance (%) explained by these modes and their temporal correlations with the decadal ENSO modulation index are listed in Table 2. The temporal correlations are statistically significant at 99% in all six CGCMs. The GFDL CM2.1 and MIUB ECHOG simulated the ENSO-induced TPDV as the first leading mode of TPDV, with more than 50% of the variance explained by this mode. In the other models (CCSM3.0, GFDL CM2.0, IPSL CM4, and MRI2.3), ENSO-induced TPDV is either the second or third mode of TPDV, explaining less than 30% of the decadal variance. When we consider another index for ENSO amplitude modulation such as N3Var index (Cibot et al. 2005), the temporal correlations are not significantly changed.

The third column of Fig. 2 demonstrates that the first mode in the decadal EOF analysis is not an ENSO-induced mode. In the cases of GFDL CM2.1 and MIUB ECHOG, this mode is the second leading mode of the EOF analysis, and the first EOF mode is the ENSO-induced TPDV. In the cases of CCSM3.0, GFDL CM2.0, IPSL CM4, and MRI2.3, this mode is the first leading mode from the EOF analysis. It should be noted that, in the GFDL CM2.0, the first and second modes described the same decadal variability because the second EOF mode represented the transition phase of the first EOF

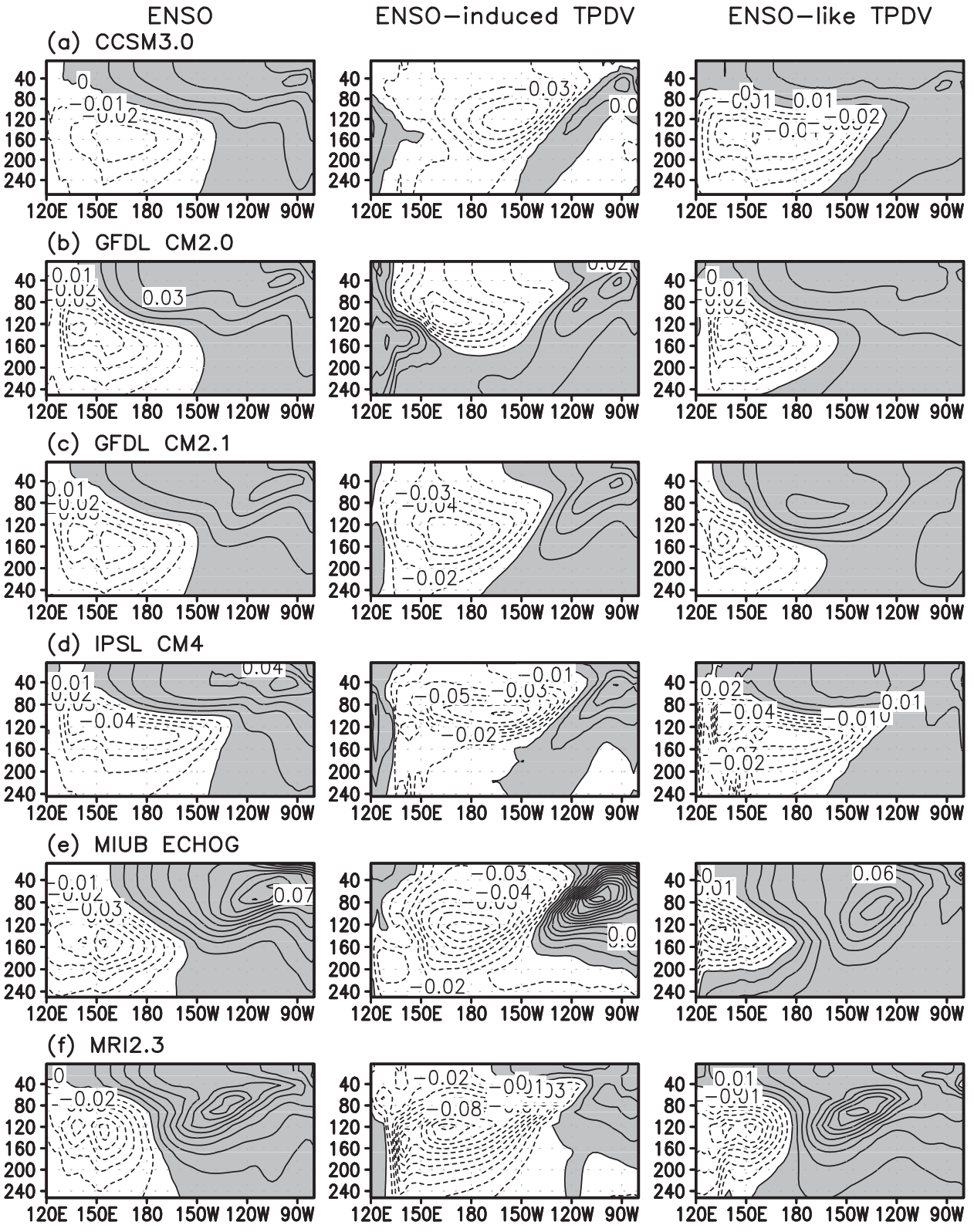

FIG. 2. Longitude–depth cross section of EOF associated with ENSO, ENSO-induced TPDV, and ENSO-like TPDV modes.

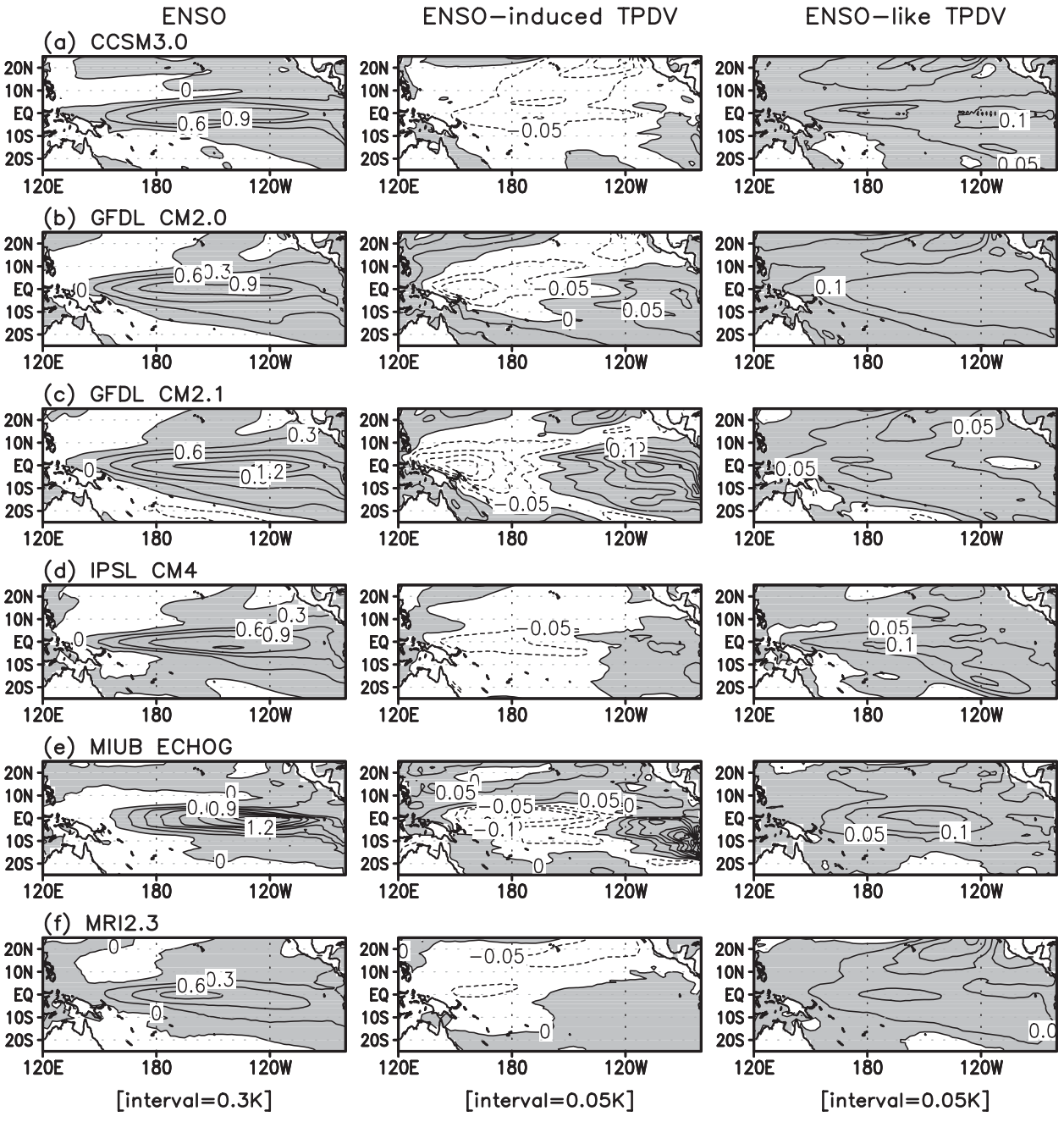

FIG. 3. Regressed map of SST associated with the EOF PC time series of ENSO, ENSO-induced TPDV, and ENSO-like TPDV modes (K).

mode. All of the modes shown in the third column of Fig. 2 have a vertical structure similar to that shown for the ENSO (i.e., the first column of Fig. 2). The pattern correlations between these two columns of Fig. 2 are 0.90 for CCSM3.0, 0.97 for GFDL CM2.0, 0.73 for GFDL CM2.1, 0.92 for IPSL CM4, 0.80 for MIUB ECHOG, and 0.92 for MRI2.3. Therefore, we identified this mode to be the ENSO-like TPDV. This mode has a structure similar to ENSO, but the centers of warm anomalies move to the west compared to those of ENSO. The center of the subsurface temperature anomalies of ENSO-like TPDV is located farther west than in the ENSO mode. The ENSO-like TPDV plays an important role in the stratification of the central Pacific, as exhibited by opposite anomalies between the surface and subsurface. The temporal correlations

between the PCs of these modes and the decadal ENSO modulation index are listed in Table 2. The ENSO-like TPDV has a weak or no relationship with the decadal modulation of ENSO amplitude, despite their similar spatial structures. This result is consistent with the result of Yeh and Kirtman (2004).

To avoid the possibility that the obtained results were caused by the decomposition process of TPDV through filtering or EOF analysis, we projected original subsurface temperature anomalies for the ENSO-induced (or ENSO-like) TPDV mode to designate a new PC time series. We then removed the high-frequency variability from this new PC time series with a 10-yr sliding average and caudated the temporal correlation between the low-pass filtered new PC and the decadal ENSO modulation index. The results were not significantly changed. This sensitivity test confirmed that the decadal variability of the east–west dipole structure was highly related to the decadal modulation of ENSO amplitude, and that there is no relationship between the amplitude modulation and decadal variability of the ENSO-like structure.

The tropical Pacific SST anomalies regressed onto the PCs of the ENSO-induced and ENSO-like modes of TPDV for all the six CGCMs (Fig. 3, second and third column). For the ENSO-like TPDV (Fig. 3, third column), the center of the SST anomaly shifted to the west compared with that of ENSO. While most of the ENSO SST anomalies were concentrated at the equator, the SST variability of the ENSO-like TPDV increased at midlatitude (not shown). This result was consistent with that of a previous study (Zhang et al. 1997). Furthermore, the positive SST anomalies of the ENSO-like TPDV mode expanded farther to the far western Pacific compared with those in the ENSO mode. As for the ENSO-induced TPDV (Fig. 3, second column), the SST anomalies were dominated by a distinctive dipole structure along the equator for all the six CGCMs. The negative anomalies in the CGCMs (except the MIUB ECHOG) expanded to the eastern subtropical region. The observation also shows the existence of such a meridionally asymmetric structure in a decadal variability mode [see Fig. 10 in Sun and Yu (2009)]. The amplitude of the SST anomaly was distinctive, especially in GFDL CM2.1 and MIUB ECHOG. The dipole-like surface structure can modify the air–sea coupling strength over the eastern and western tropical Pacific in opposite ways, as suggested by Choi et al. (2011). A warmer mean surface condition can allow anomalous convection to be more easily induced by an SST anomaly, thus leading to enhanced air–sea coupling, and vice versa for a colder mean surface condition. As a result, the positive phase of the zonal-dipole structure can lead to a reduced zonal gradient in the mean SST and stronger amplitude of ENSO, and vice versa for the negative phase of the dipole mode. In addition to affecting the air–sea coupling strength, the dipole structure also controls the contribution of oceanic feedback to the spatial distribution of ENSO (Choi et al. 2011). The centers of the SST anomalies for El Niño and La Niña are also modulated by the dipole-like decadal variability. For instance, the eastern (central) Pacific type of El Niño and the central (eastern) Pacific type of La Niña (Yu and Kao 2007; Ashok et al. 2007; Kao and Yu 2009; Kug et al. 2009) occur more frequently during the weak (strong) gradient of mean SST for the ENSO-induced TPDV. Choi et al. (2011, 2012) provide a detailed mechanism of how the zonal-dipole surface conditions modulate the amplitude and spatial pattern of ENSO.

4. Relationship between two types of TPDVs and ENSO

In this section, we discuss the relationships between ENSO and two types of TPDVs. Based on evidence identified in the previous section, three specific associations are discussed: (a) between the ENSO-induced TPDV and the two-way ENSO–mean state interactions, (b) between the ENSO-like TPDV and the recharged oscillator of ENSO, and (c) between the intensity ratio of two types of TPDV and the ENSO characteristics in the CGCMs.

a. ENSO-induced TPDV and ENSO residuals

As mentioned in the introduction, the asymmetry between El Niño and La Niña can lead to residuals that slowly modify the tropical Pacific mean state. This residual effect of ENSO asymmetries has been demonstrated in both observations (An 2004; Sun and Yu 2009; McPhaden et al. 2011) and model simulations (Rodgers et al. 2004; Schopf and Burgman 2006; Choi et al. 2012; Yu and Kim 2011). In the present study, we examine the characteristics of ENSO events, ENSO residuals, and their relationships with ENSO-induced TPDV.

To define El Niño and La Niña events, we used the modified Niño-3 and Niño-4 indices, referred to as NIÑO3m and NIÑO4m in this study because the cold tongue in most CGCMs is strongly developed compared with that of observation (Kug et al. 2010; Choi et al. 2011, 2012). NIÑO3m SSTA (the averaged SST anomaly over 5°S–5°N, 170°–110°W) and NIÑO4m SSTA (the averaged SST anomaly over 5°S–5°N, 140°E–170°W) shifted about 20° west in longitude compared with the conventional definition. El Niño (La Niña) events are defined as events that have NIÑO3m or NIÑO4m indices greater (less) than 0.5°C (−0.5°C) during the

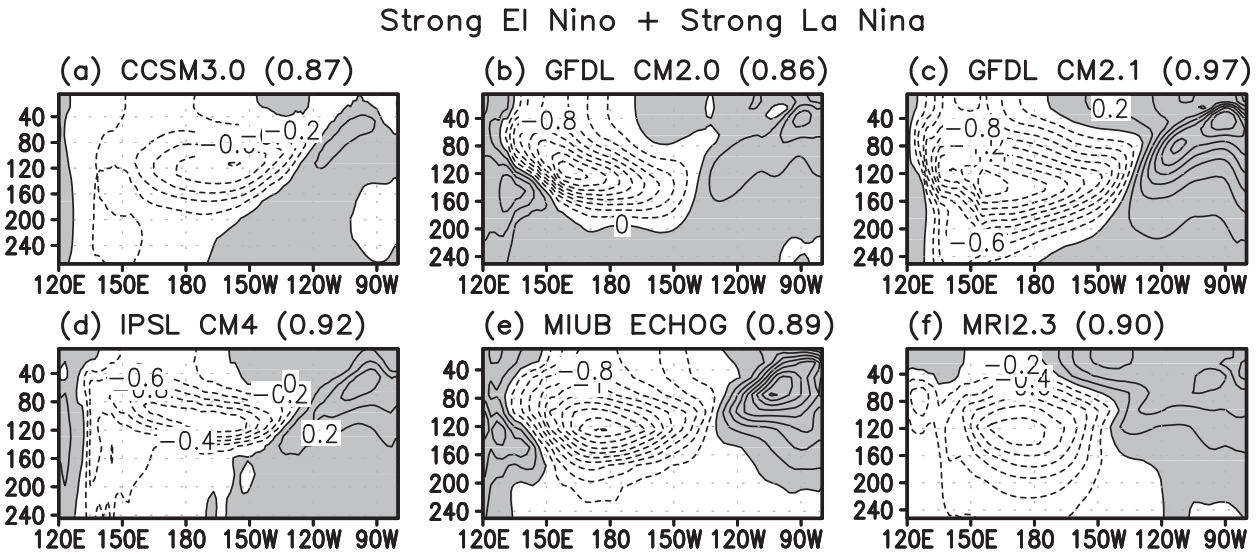

FIG. 4. Residuals induced by El Niño–La Niña during the strong ENSO period. The parentheses in the upper right represent the spatial correlation between the residuals and the EOF pattern of ENSO-induced TPDV. The contour interval is 0.2 K.

boreal winter [D(0)JF(1), where winter is defined as December–February (DJF)]. Only in the case of MRI2.3, normalized NIÑO3m and NIÑO4m indices are used because its ENSO amplitudes are relatively small compared to those of the other five CGCMs. The anomalies during El Niño and La Niña winters [D(0)JF(1)] are composited with respect to the ENSO-induced TPDV phase. The strong (weak) period is the period when the normalized PC time series of the ENSO-induced TPDV yields a standard deviation greater (less) than 0.5 (−0.5). Since ENSO-induced TPDV is highly correlated with the amplitude modulation of ENSO, the state of the climate is linked to a strong ENSO period that corresponds to the positive phase of ENSO-induced TPDV (Fig. 2, second column). On the other hand, the state of the climate associated with a weak ENSO period is opposite to the pattern expressed in the second column of Fig. 2.

Residuals induced by the spatial asymmetry between El Niño and La Niña are calculated by simply adding El Niño and La Niña composites during boreal winter [D(0)JF(1)]. Figure 4 shows the residuals induced by ENSO asymmetries during the strong ENSO period for the six selected CGCMs. Overall, there is an east–west contrast pattern similar to the pattern of the ENSO-induced TPDV. The parentheses shown in each panel indicate the spatial correlation between the residual pattern and the EOF pattern of ENSO-induced TPDV. All CGCMs demonstrate strong similarity in the spatial pattern, with a correlation coefficient of more than 0.85. ENSO residuals during the weak ENSO period are shown in Fig. 5. In the case of GFDL CM2.0, the zonal dipole structure appears to be collapsed. However, a general east–west dipole structure also exists in the other five CGCMs, as demonstrated in Fig. 4, but with a smaller magnitude. These models also demonstrate a large negative spatial correlation between ENSO residuals during the weak ENSO period and EOF patterns of ENSO-induced TPDV.

b. Phase transitions of ENSO-like TPDV and ENSO

According to the recharge oscillator theory, the eastward (westward) gradient of heat content conduces poleward (equatorial) transport by meridional divergence (convergence) of the geostrophic currents (Jin 1997a,b; Meinen and McPhaden 2001; Kug et al. 2003). The lagged regression of ocean heat content against the PC time series of the ENSO mode from the six CGCMs is shown in Fig. 6. The heat content is defined as the temperature anomalies vertically integrated from the surface to a depth of 300 m. The lagged months correspond to three, six, and nine months after the mature phase. Lag 0 represents the mature phase of the El Niño events. Typically, ocean heat content anomalies accumulate over the eastern tropical Pacific during the mature phase, three months after which the heat content anomalies start to be transported to the off-equator region. The northward transport is remarkably stronger than the southward transport in four of the CGCMs: CCSM3.0, GFDL CM2.0, GFDL CM2.1, and IPSL CM4. In the other two models (MIUB ECHOG and MRI2.3), the northward exchange of heat content is twice as strong as the southward exchange. This hemispherically asymmetric discharge process is due to the southward shift of zonal wind stress from the equator (Kug

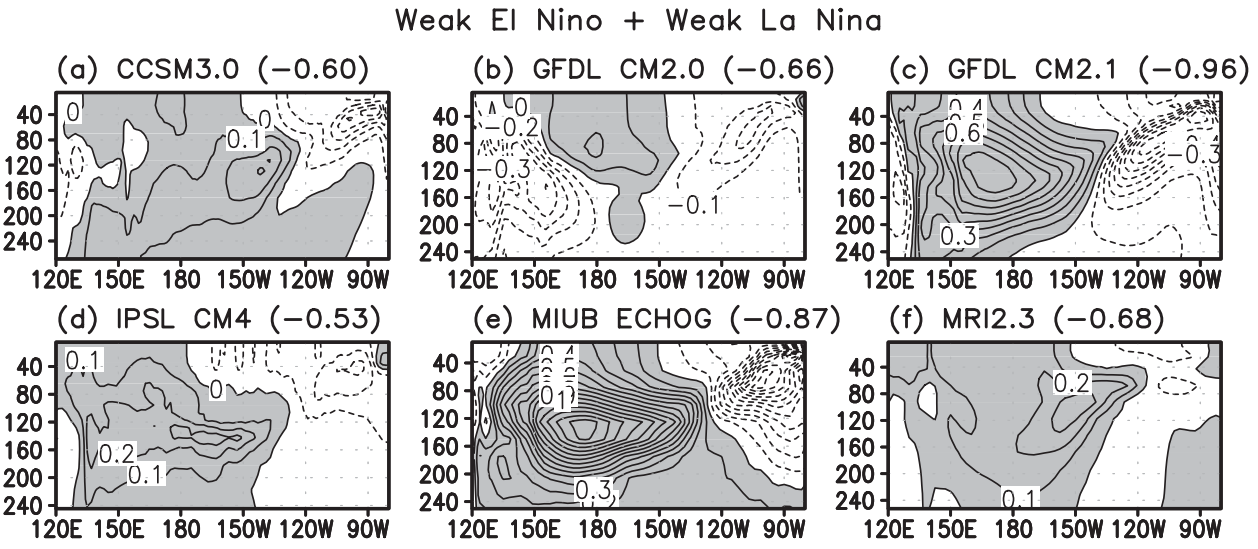

FIG. 5. Residuals induced by El Niño–La Niña during the weak ENSO period. The contour interval is 0.1 K.

et al. 2003, 2010). Six months after maturity, the negative heat content anomalies emerge in the western and central tropical Pacific. Eventually, the equatorial heat content is totally discharged from the equator to the off-equatorial region, as shown in the lag +9 figures. In the case of MRI2.3, the amplitude of the discharged equatorial heat content is small. This is because the center of the ENSO SST anomalies in MRI2.3 is located farther west than in the other models (Fig. 3f). Kug et al. (2010) suggested that the discharge mechanism depended on the longitudinal location of the SST anomalies and the heat content distribution. The study indicated that the discharge becomes more effective the farther east the SST anomaly center is located in the GFDL CM2.1 model.

To examine the discharge process for ENSO-like TPDV, we performed the same regression analysis with the PC time series of the ENSO-like TPDV mode (Fig. 7). Ocean content anomalies accumulate over the eastern Pacific at the mature phase (see figures marked +0yr) and later propagate to the off-equator region (Fig. 7). The northward transport is also larger than the southward transport in all models except MIUB ECHOG. Following the transport of positive anomalies to the off-equator region, negative ocean heat content anomalies propagate from the west to the east over the tropical Pacific. In the case of GFDL CM2.1, IPSL CM4, and MRI2.3, the negative anomaly over the western tropical South Pacific is remarkably larger than that over the North Pacific region. This result is similar to that reported by Luo and Yamagata (2001), who suggested that the air–sea interaction in the western tropical South Pacific is a key region for understanding ENSO-like TPDV. It appears that the phase change from positive to negative for the ENSO-like TPDV mode occurs more abruptly over the equatorial Pacific as compared with ENSO. This indicates that the time scale for the ENSO-like TPDV transition is irregular in the selected CGCMs. The results presented in Fig. 7 are consistent with those reported by Knutson and Manabe (1998), Vimont et al. (2002), Luo et al. (2003), and Wang et al. (2003), who argued that the ENSO-like TPDV has a ''delayed oscillator'' mechanism that bears similarity to the ENSO time scale.

c. *ENSO-induced and ENSO-like TPDVs*

If ENSO-induced and ENSO-like TPDVs are physically the same mode but in different phases, their dominant period should be similar with a distinctive lead–lag relationship between them. Figure 8 shows the normalized power spectrum of the PCs of two TPDV modes from a spectral analysis. In the case of four CGCMs (CCSM3.0, IPSL CM4, MIUB ECHOG, and MRI2.3), the maximum periods of ENSO-induced TPDV are not well matched to those of ENSO-like TPDV, but the general spectra in their decadal-to-interdecadal bands are quite similar. The other two models—GFDL CM2.0 and GFDL CM2.1—have a similar dominant period in both ENSO-induced and ENSO-like TPDVs. The results are inconsistent among the six CGCMs with respect to the lead–lag relationship between the two types of TPDVs (not shown). In two CGCMs—GFDL CM2.1 and MIUB ECHOG—a statistically significant negative lead–lag relationship was detected between two types of TPDVs at a 95% confidence level. These associations appeared to result from the transition patterns of ENSO-like TPDV. The dipole-like structure appears during the transition phase of ENSO-like TPDV

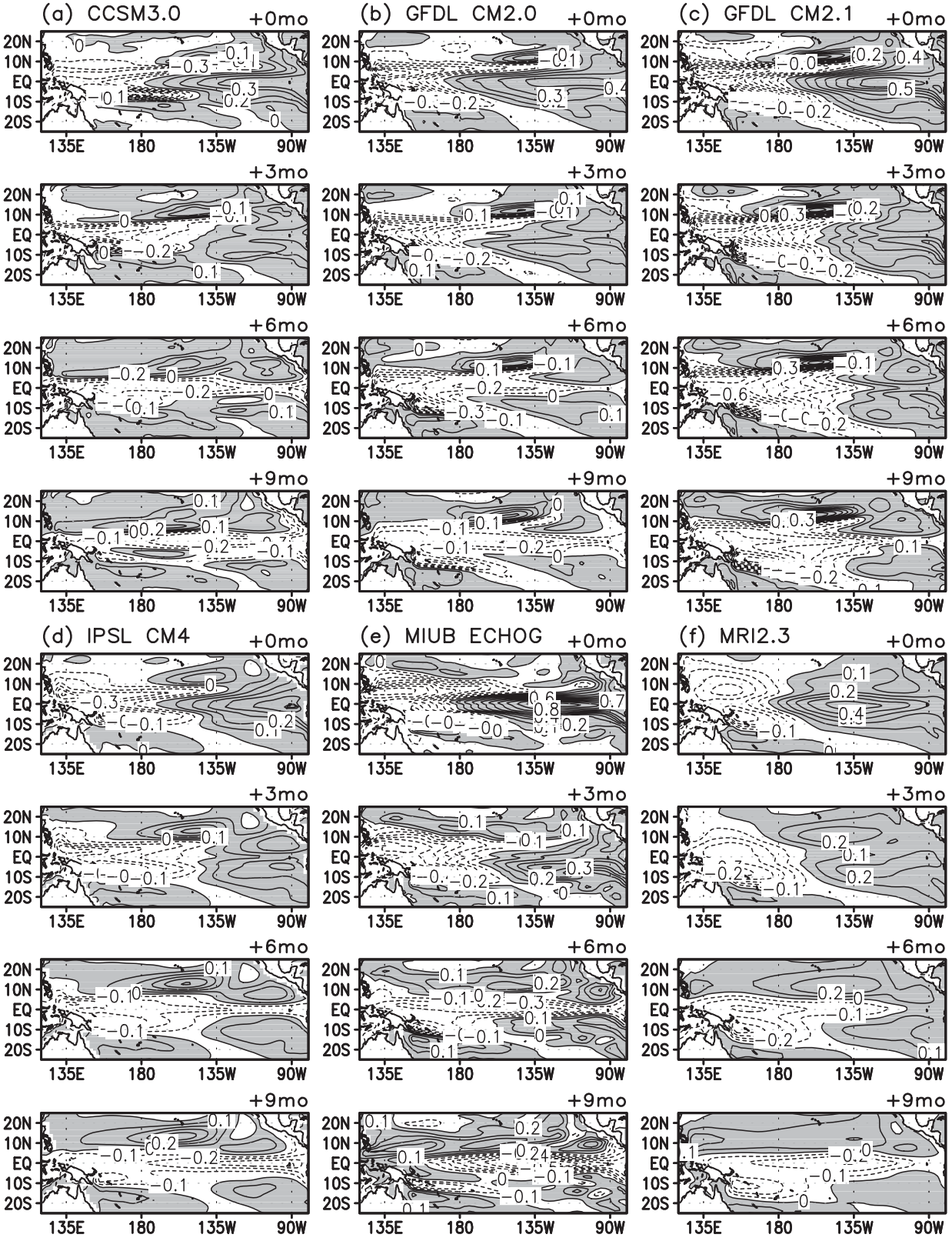

FIG. 6. Lagged regression map of the ocean heat content for ENSO mode. The heat content is defined as the vertically integrated temperature from the surface to a depth of 300 m. The contour interval is 0.1 K.

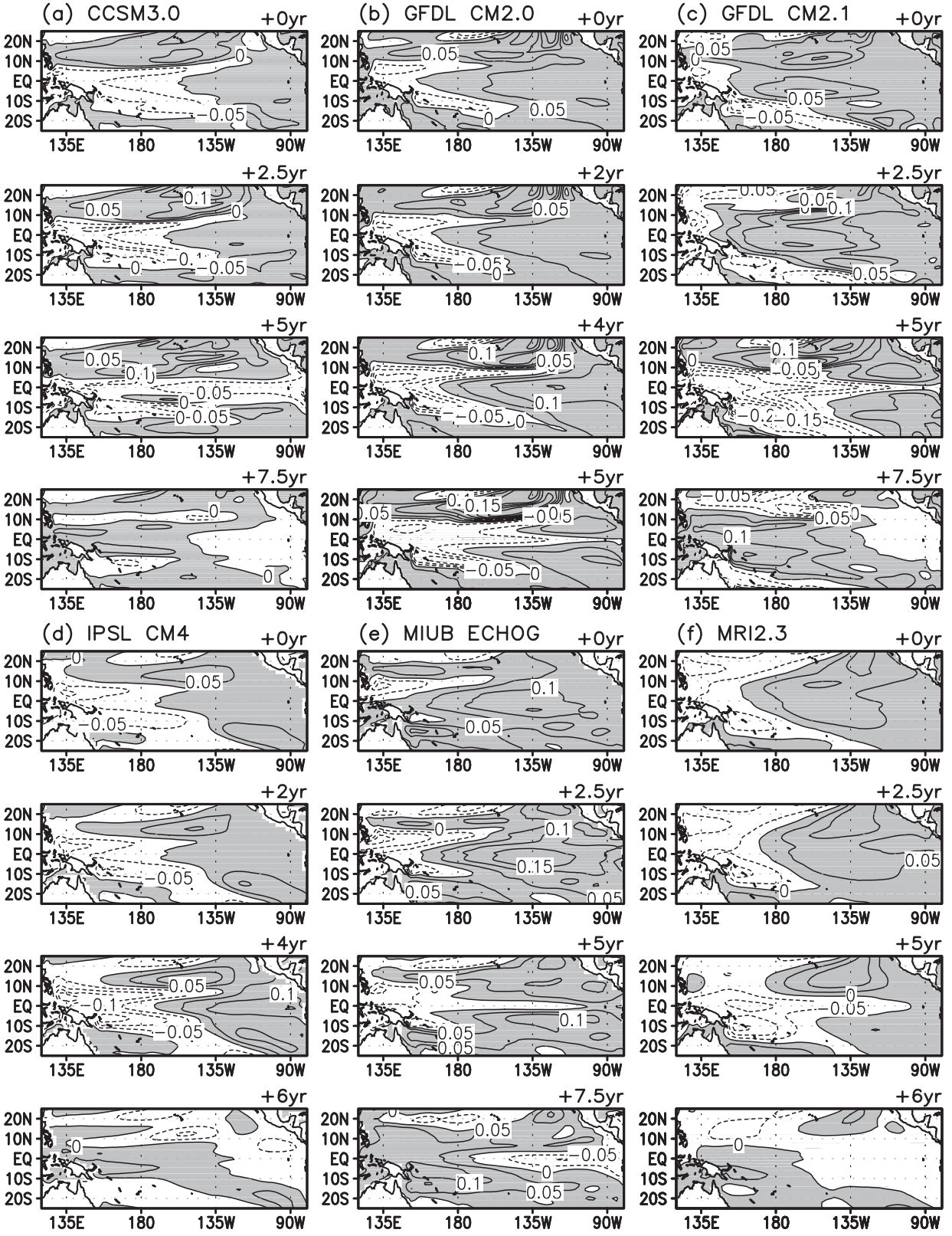

FIG. 7. Lagged regression map of the ocean heat content for ENSO-like TPDV. The contour interval is 0.05 K.

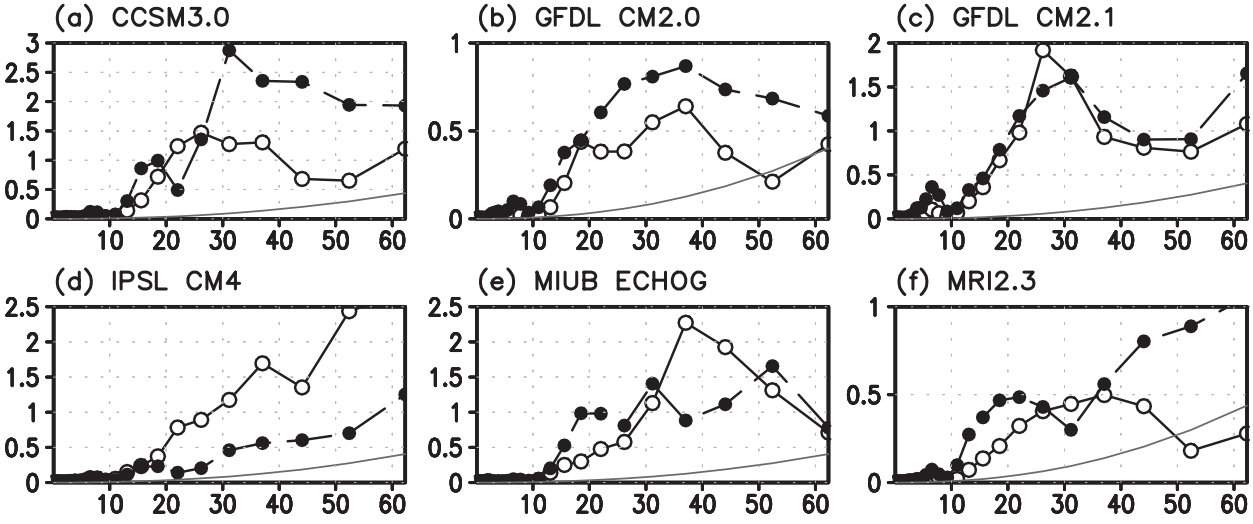

FIG. 8. Normalized power spectrum of the EOF PC time series. The *x* axis indicates the period (year). The solid (with open circle) and dashed (with closed circle) lines indicate the ENSO-induced and ENSO-like TPDVs, respectively. The thin solid line is the 95% significance level.

(Fig. 7), where the last panel of each model shows an east–west dipole-like distribution of heat content along the equator. This is known as the negative mature phase of ENSO-induced TPDV. Thus, the transition of ENSO-like TPDV could impact the mature phase of ENSO-induced TPDV. Similarly, Choi et al. (2012) demonstrated the possibility that ENSO-like TPDV promotes the phase transition of ENSO-induced TPDV by modifying the stratification in the GFDL CM2.1 simulation (in their Fig. 12). Consequently, these results potentially suggest that the two types of TPDVs are not the same physical modes. Their phases are linked to each other despite the possibility of different growing mechanisms.

Meanwhile, if the ENSO-induced TPDV interplays with decadal change in the asymmetry of El Niño–La Niña, their strong interaction enhances both ENSO-induced TPDV and residuals due to El Niño–La Niña asymmetry (An 2004; Choi et al. 2009, 2012). To understand this interaction quantitatively, we analyzed the relationship between amplitudes of ENSO-induced TPDV and the ENSO residuals. The amplitude of residuals in each model was measured as a spatial correlation in a residual pattern between strong and weak ENSO periods (Figs. 4 and 5). The stronger and more symmetric residual effects were expected to yield a larger spatial correlation. In addition, an enhanced ENSO-induced TPDV via a strong residual effect could be expected for the larger spatial correlation. Therefore, the spatial correlation in the residual pattern between the strong and weak ENSO periods is one representative value of the strength of the two-way interaction between ENSO residuals and ENSO-induced TPDV.

The *x* axis in Figs. 9a and 9b is the spatial correlation in the residual pattern between the strong and weak ENSO periods. The *y* axis in Figs. 9a and 9b represents the EOF variance of ENSO-induced and ENSO-like TPDVs, respectively. The scatterplots indicate the results calculated from the six selected CGCMs. The correlation between *x* and *y* in Fig. 9a is −0.87 whereas this correlation is 0.95 in Fig. 9b. Both correlations are statistically significant at the 95% confidence level. Note in Fig. 9b the overlap of the points for CCSM3.0 and MRI2.3, which have a similar spatial correlation (approximately 0.59) and variance. The negative relationship in Fig. 9a indicates that the ENSO-induced TPDV would be intensified with an enhanced relationship between ENSO residuals and ENSO-induced TPDV. This supports the finding that interactive feedback between ENSO and the mean state contributes to low-frequency variability, or ENSO-induced TPDV (Sun and Yu 2009; Choi et al. 2009). The positive relationship in Fig. 9b also implies that low-frequency variability related to ENSO-like TPDV is reduced as the interactive feedback between ENSO and mean state (or the variance of ENSO-induced TPDV) is enhanced. Consequently, the strong two-way feedback between ENSO and the tropical Pacific mean state intensifies the ENSO-induced TPDV (i.e., dipole-like structure) while it reduces the ENSO-like TPDV (i.e., triangular structure). Therefore, the variance ratio between the two types of TPDV in each CGCM depends on the strength of the feedback between ENSO and the tropical Pacific mean state in each model.

The symmetry between strong and weak ENSO residuals, indicating a connection between ENSO and

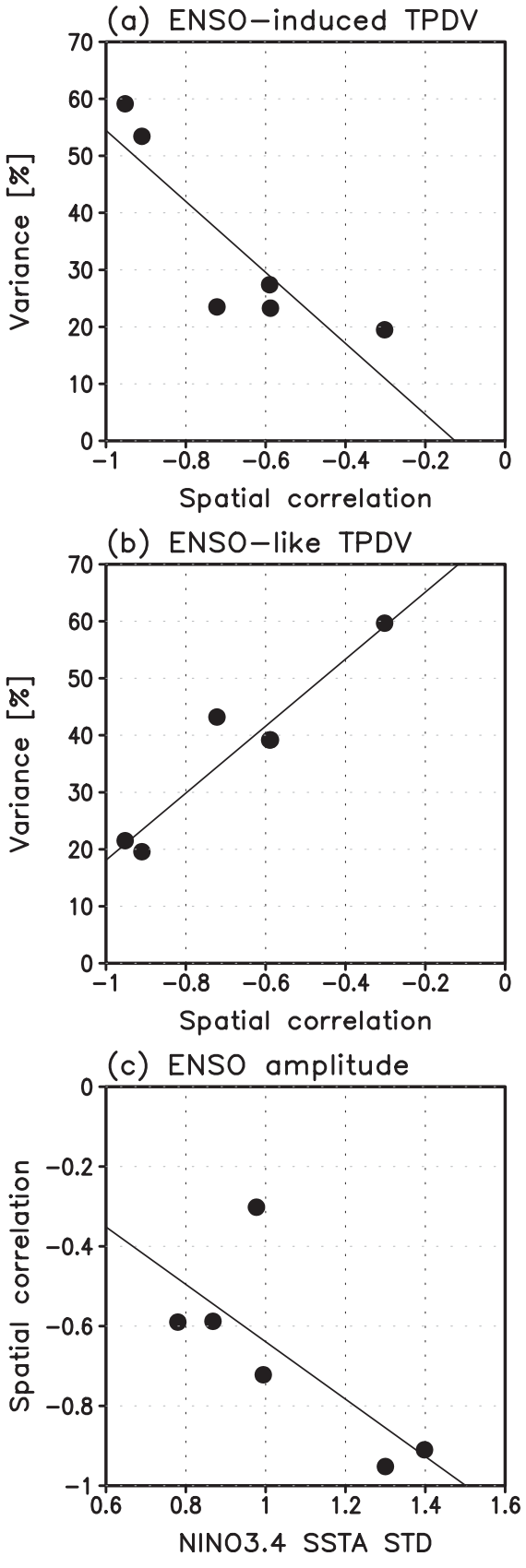

ENSO-induced TPDV, appears to be related to ENSO variability. The *x* axis in Fig. 9c represents the standard deviation of the Niño-3.4 SST anomaly index (Table 1). The *y* axis refers to the spatial correlation depicted by the *x* axis in Figs. 9a and 9b. The correlation between the *x* and *y* variables is −0.73, which is statistically significant at the 90% confidence level (Fig. 9c). Thus, the two-way feedback between ENSO and ENSO-induced TPDV tends to be stronger as the ENSO variability grows. This indicates the possibility that the CGCMs generating strong ENSO could effectively simulate the characteristics of El Niño–La Niña events linked to changes in the tropical Pacific mean state. On the other hand, the CGCMs, which have a relatively weak ENSO variability amplitude, simulate a weak interactive feedback mechanism between ENSO and the tropical Pacific mean state due to the small diversity of ENSO types. As a result, the simulated large ENSO creates strong interactive feedback between ENSO and the tropical Pacific mean state in most cases, leading to intensified ENSO-induced TPDV and reduced ENSO-like TPDV modes in CGCMs. The amplitude of ENSO is affected by a variety of factors, including the simulated tropical Pacific climate state, convective parameterization, air–sea net flux interaction, ocean current schemes, and more. Therefore, these subjects should be further investigated in future studies.

5. Summary and discussion

In this study, we analyzed the outputs of long-term CMIP3 CGCM simulations to examine the relationship between ENSO and two leading modes of TPDV. We selected for analysis six CGCMs (CCSM3.0. GFDL CM2.0, GFDL CM2.1, IPSL CM4, MIUB ECHOG, and MRI2.3) that reasonably simulate the climate state of the tropical Pacific, ENSO, and TPDVs. We confirmed that the leading variability mode on interannual time scales was ENSO in all selected CGCMs. The six selected models effectively simulated equatorially confined SST variability and basin-scale subsurface variations during El Niño events. We then separated the two

←

FIG. 9. Scatterplots in the spatial correlation–variance domain. The *x* axis indicates the spatial correlation between ENSO-induced residuals during the strong and weak ENSO periods. The *y* axes refer to the variance (%) of (a) ENSO-induced TPDVs, (b) ENSO-like TPDVs, and (c) scatterplots of the standard deviation of the Niño-3.4 SSTA index–spatial correlation. Closed circles indicate the six CGCMs listed in Table 2. The slope of the thin lines corresponds to the linear regression coefficient.

modes of TPDV by applying an EOF analysis to the low-pass filtered subsurface temperature anomalies at the equator. The first mode was the ENSO-induced TPDV, which is related to the decadal ENSO amplitude modulation. The PC time series of the ENSO-induced TPDV was highly correlated with the 10-yr sliding standard deviation of the Niño-3.4 SST anomaly. The spatial pattern of ENSO-induced TPDV exhibits an east–west zonal contrast (dipole-like) pattern in its surface and subsurface structures. The other mode was the ENSO-like TPDV, which shows a triangular SST structure similar to ENSO but with a wider meridional extension. There was a weak relationship between the PC time series of the ENSO-like TPDV and the decadal modulation index of ENSO amplitude. The ENSO-like TPDV showed a basin-scale, triangular pattern of SST variations, but the center of SST anomalies is weaker than the ENSO and locates farther west. This mode of decadal variability is characterized by an east–west zonal contrast in its subsurface structure, indicating that the effects of this mode on stratification were increased over the western tropical Pacific.

With regard to the growth mechanism, the ENSO-induced TPDV was related to the ENSO residuals resulting from the spatial asymmetry between El Niño and La Niña. The asymmetry in El Niño–La Niña leaves a residual effect in the background state, which gradually accumulates and gives rise to the ENSO-induced TPDV. The high simultaneous correlation between the ENSO-induced TPDV and the decadal modulation index of ENSO amplitude and the strong resemblance between the ENSO residual pattern and the pattern of the ENSO-induced TPDV in the six CGCMs indicate that these two phenomena strongly interact with each other. Meanwhile, this interaction seems to be shown in observation. We note that McPhaden et al. (2011) addressed the relationship between the recent more frequent occurrence of central Pacific El Niño and the changes in the background state, which is regarded as the negative phase of ENSO-induced TPDV in this study. On the other hand, a slower recharge/discharge oscillator works on a decadal-to-interdecadal time scale, causing ENSO-like TPDV in CGCMs. The transport of heat content from the equator to the off-equator follows the peak of ENSO-like TPDV. Meanwhile, the dominant periods of two types of TPDVs are quite similar even though their growing mechanisms are different, which appears to be related to the linkage between their phases. The transition phase of ENSO-like TPDV has a dipole-like structure at the equator that is similar to the mature phase of ENSO-induced TPDV. Therefore, the mature phase of ENSO-induced TPDV tends to be locked into the transition phase of ENSO-like TPDV, which could result in similar periods.

In addition, we compared the variance ratio between the two types of TPDV in each CGCM and the strength of interactive feedback between ENSO and the tropical Pacific mean state. The results support the notion that these two TPDVs have different growing mechanisms. When the two-way feedback between ENSO residuals and ENSO-induced TPDV strengthens, the variance of the ENSO-induced TPDV was found to increase but the variance of the ENSO-like TPDV decreases. The two-way feedback between ENSO residuals and ENSO-induced TPDV appears to depend on ENSO variability in CGCMs. With respect to changes in the tropical Pacific mean state, the characteristics of El Niño–La Niña were well simulated when the ENSO variability grew larger in CGCMs. As a result, the larger ENSO variability in CGCMs, the stronger interactive feedback between ENSO and the tropical Pacific mean state leads to an intensified ENSO-induced TPDV and a weakened ENSO-like TPDV mode in CGCMs. It should be noted that this two-way feedback works well for eastern Pacific El Niño than central Pacific El Niño because of its strong asymmetry (An et al. 2005). In this regard, we could expect that an increased occurrence of central Pacific El Niño during the recent decades (Ashok et al. 2007; Yeh et al. 2009) or the relative weakening of eastern Pacific El Niño variability [this alternation was argued by Choi et al. (2012)] presumably results in the intensified ENSO-like TPDV and the weakened ENSO-induced TPDV. This point needs to be pursued in the future.

Although we proposed a possible relationship between ENSO-induced TPDV and ENSO-like TPDV, particularly a variance ratio between the two TPDVs, the physical mechanism was not fully addressed in this study. Furthermore, the basis for the lack of relationship between ENSO-like TPDV and the decadal ENSO modulation is not clear, even though the structure of ENSO-like TPDV is only different on the surface from ENSO-induced TPDV. Additionally, problems associated with global warming should be discussed in future studies. In the future, the ENSO amplitude is likely to be affected by the changed mean state. Thus, an understanding of two types of tropical Pacific decadal variability is essential for improving the predictability of future ENSO. A more comprehensive study of the physical linkage between two types of TPDV and sensitivity tests will be necessary in the near future.

Acknowledgments. This work was funded by the Korea Meteorological Administration Research and Development Program under Grant CATER 2012-3043.

REFERENCES

AchutaRao, K. M., and K. R. Sperber, 2002: Simulation of the El Niño–Southern Oscillation: Results from the Coupled Model Intercomparison Project. *Climate Dyn.,* **19,** 191–209.

An, S.-I., 2004: Interdecadal change in the El Niño–La Niña asymmetry. *Geophys. Res. Lett.,* **31,** L23210, doi:10.1029/2004GL021699.

——, 2009: A review of interdecadal changes in the nonlinearity of the El Niño–Southern Oscillation. *Theor. Appl. Climatol.,* **97,** 29–40.

——, and B. Wang, 2000: Interdecadal change of the structure of the ENSO mode and its impact on the ENSO frequency. *J. Climate,* **13,** 2044–2055.

——, Y.-G. Ham, J.-S. Kug, F.-F. Jin, and I.-S. Kang, 2005: El Niño–La Niña asymmetry in the Coupled Model Intercomparison Project simulations. *J. Climate,* **18,** 2617–2627.

——, Z. Ye, and W. W. Hsieh, 2006: Changes in the leading ENSO modes associated with the late 1970s climate shift: Role of surface zonal current. *Geophys. Res. Lett.,* **33,** L14609, doi:10.1029/2006GL026604.

Ashok, K., S. K. Behera, S. A. Rao, H. Weng, and T. Yamagata, 2007: El Niño Modoki and its teleconnection. *J. Geophys. Res.,* **112,** C11007, doi:10.1029/2006JC003798.

Bejarano, L., and F.-F. Jin, 2008: Coexistence of equatorial coupled modes of ENSO. *J. Climate,* **21,** 3051–3067.

Burgman, R. J., P. S. Schopf, and B. P. Kirtman, 2008: Decadal modulation of ENSO in a hybrid coupled model. *J. Climate,* **21,** 5482–5500.

Carton, J. A., and B. S. Giese, 2008: A reanalysis of ocean climate using Simple Ocean Data Assimilation (SODA). *Mon. Wea. Rev.,* **136,** 2999–3017.

——, ——, and S. A. Grodsky, 2005: Sea level rise and the warming of the oceans in the Simple Ocean Data Assimilation (SODA) ocean reanalysis. *J. Geophys. Res.,* **110,** C09006, doi:10.1029/2004JC002817.

Choi, J., S.-I. An, B. Dewitte, and W. W. Hsieh, 2009: Interactive feedback between the tropical Pacific decadal oscillation and ENSO in a coupled general circulation model. *J. Climate,* **22,** 6597–6611.

——, ——, J.-S. Kug, and S.-W. Yeh, 2011: The role of mean state on changes in El Niño's flavor. *Climate Dyn.,* **37,** 1205–1215.

——, ——, and S.-W. Yeh, 2012: Decadal amplitude modulation of two types of ENSO and its relationship with the mean state. *Climate Dyn.,* **38,** 2631–2644.

Cibot, C., E. Maisonnave, L. Terray, and B. Dewitte, 2005: Mechanisms of tropical Pacific interannual-to-decadal variability in the ARPEGE/ORCA global coupled model. *Climate Dyn.,* **24,** 823–842.

Collins, M., and Coauthors, 2010: The impact of global warming on the tropical Pacific Ocean and El Niño. *Nat. Geosci.,* **3,** 391–397.

Dewitte, B., S.-W. Yeh, B.-K. Moon, C. Cibot, and L. Terray, 2007: Rectification of the ENSO variability by interdecadal changes in the equatorial background mean state in a CGCM simulation. *J. Climate,* **20,** 2002–2021.

——, S. Thual, S.-W. Yeh, S.-I. An, B.-K. Moon, and B. S. Giese, 2009: Low-frequency variability of temperature in the vicinity of the equatorial Pacific thermocline in SODA: Role of equatorial wave dynamics and ENSO asymmetry. *J. Climate,* **22,** 5783–5795.

Evans, M. N., A. Kaplan, and M. A. Cane, 2002: Pacific sea surface temperature field reconstruction from coral δ^{18}O data using reduced space objective analysis. *Paleoceanography,* **17,** 1007, doi:10.1029/2000PA000590.

Fedorov, A. V., and S. G. H. Philander, 2000: Is El Niño changing? *Science,* **288,** 1997–2002.

——, and ——, 2001: A stability analysis of tropical ocean–atmosphere interactions: Bridging measurements and theory for El Niño. *J. Climate,* **14,** 3086–3101.

Flügel, M., and P. Chang, 1999: Stochastically induced climate shift of El Niño–Southern Oscillation. *Geophys. Res. Lett.,* **26,** 2473–2476.

Garreaud, R., and D. S. Battisti, 1999: Interannual (ENSO) and interdecadal (ENSO-like) variability in the Southern Hemisphere tropospheric circulation. *J. Climate,* **12,** 2113–2123.

Hannachi, A., D. Stephenson, and K. Sperber, 2003: Probability-based methods for quantifying nonlinearity in the ENSO. *Climate Dyn.,* **20,** 241–256.

Imada, Y., and M. Kimoto, 2009: ENSO amplitude modulation related to Pacific decadal variability. *Geophys. Res. Lett.,* **36,** L03706, doi:10.1029/2008GL036421.

Jin, F.-F., 1997a: An equatorial ocean recharge paradigm for ENSO. Part I: Conceptual model. *J. Atmos. Sci.,* **54,** 811–829.

——, 1997b: An equatorial ocean recharge paradigm for ENSO. Part II: A stripped-down coupled model. *J. Atmos. Sci.,* **54,** 830–847.

——, J. D. Neelin, and M. Ghil, 1994: El Niño on the devil's staircase: Annual subharmonic steps to chaos. *Science,* **264,** 70–72.

Kao, H. Y., and J.-Y. Yu, 2009: Contrasting eastern-Pacific and central-Pacific types of ENSO. *J. Climate,* **22,** 615–632.

Kirtman, B. P., and P. S. Schopf, 1998: Decadal variability in ENSO predictability and prediction. *J. Climate,* **11,** 2804–2822.

Knutson, T. R., and S. Manabe, 1998: Model assessment of decadal variability and trends in the tropical Pacific Ocean. *J. Climate,* **11,** 2273–2296.

Kug, J.-S., I.-S. Kang, and S.-I. An, 2003: Symmetric and antisymmetric mass exchanges between the equatorial and off-equatorial Pacific associated with ENSO. *J. Geophys. Res.,* **108,** 3284, doi:10.1029/2002JC001671.

——, F.-F. Jin, and S.-I. An, 2009: Two types of El Niño events: Cold tongue El Niño and warm pool El Niño. *J. Climate,* **22,** 1499–1515.

——, J. Choi, S.-I. An, F.-F. Jin, and A. T. Wittenberg, 2010: Warm pool and cold tongue El Niño events as simulated by the GFDL 2.1 coupled GCM. *J. Climate,* **23,** 1226–1239.

Latif, M., R. Kleeman, and C. Eckert, 1997: Greenhouse warming, decadal variability, or El Niño? An attempt to understand the anomalous 1990s. *J. Climate,* **10,** 2221–2239.

——, and Coauthors, 2001: ENSIP: The El Niño simulation intercomparison project. *Climate Dyn.,* **18,** 255–276.

Li, J., and Coauthors, 2011: Interdecadal modulation of El Niño amplitude during the past millennium. *Nature Climate Change,* **1,** 114–118.

Luo, J.-J., and T. Yamagata, 2001: Long-term El Niño–Southern Oscillation (ENSO)-like variation with special emphasis on the South Pacific. *J. Geophys. Res.,* **106** (C10), 22 211–22 227.

——, S. Masson, S. Behera, P. Delecluse, S. Gualdi, A. Navarra, and T. Yamagata, 2003: South Pacific origin of the decadal ENSO-like variation as simulated by a coupled GCM. *Geophys. Res. Lett.,* **30,** 2250, doi:10.1029/2003GL018649.

Mantua, N. J., S. R. Hare, Y. Zhang, J. M. Wallace, and R. C. Francis, 1997: A Pacific decadal climate oscillation with impacts on salmon production. *Bull. Amer. Meteor. Soc.,* **78,** 1069–1079.

McPhaden, M. J., T. Lee, and D. McClurg, 2011: El Niño and its relationship to changing background conditions in the tropical Pacific Ocean. *Geophys. Res. Lett.,* **38,** L15709, doi:10.1029/2011GL048275.

Meehl, G. A., C. Covey, K. E. Taylor, T. Delworth, R. J. Stouffer, M. Latif, B. McAvaney, and J. F. B. Mitchell, 2007: The WCRP CMIP3 multimodel dataset: A new era in climate change research. *Bull. Amer. Meteor. Soc.,* **88,** 1383–1394.

Meinen, C. S., and M. J. McPhaden, 2001: Interannual variability in warm water volume transports in the equatorial Pacific during 1993–99. *J. Phys. Oceanogr.,* **31,** 1324–1345.

Rodgers, K. B., P. Friederichs, and M. Latif, 2004: Tropical Pacific decadal variability and its relation to decadal modulations of ENSO. *J. Climate,* **17,** 3761–3774.

Schopf, P. S., and R. J. Burgman, 2006: A simple mechanism for ENSO residuals and asymmetry. *J. Climate,* **19,** 3167–3179.

Sun, F., and J.-Y. Yu, 2009: A 10–15-yr modulation cycle of ENSO intensity. *J. Climate,* **22,** 1718–1735.

Sverdrup, H. U., M. W. Johnson, and R. H. Fleming, 1942: *The Oceans: Their Physics, Chemistry, and General Biology*. Prentice-Hall, 1087 pp.

Thual, S., B. Dewitte, S.-I. An, and N. Ayoub, 2011: Sensitivity of ENSO to stratification in a recharge–discharge conceptual model. *J. Climate,* **24,** 4332–4349.

Timmermann, A., 2003: Decadal ENSO amplitude modulations: A nonlinear paradigm. *Global Planet. Change,* **37,** 135–156.

——, J. Oberhuber, A. Bacher, M. Esch, M. Latif, and E. Roeckner, 1999: Increased El Niño frequency in a climate model forced by future greenhouse warming. *Nature,* **398,** 694–697.

Vimont, D. J., D. S. Battisti, and A. C. Hirst, 2002: Pacific interannual and interdecadal equatorial variability in a 1000-yr simulation of the CSIRO coupled general circulation model. *J. Climate,* **15,** 160–178.

Wallace, J. M., and D. S. Gutzler, 1981: Teleconnections in the geopotential height field during the Northern Hemisphere winter. *Mon. Wea. Rev.,* **109,** 784–812.

Wang, X., F.-F. Jin, and Y. Wang, 2003: A tropical ocean recharge mechanism for climate variability. Part II: A unified theory for decadal and ENSO modes. *J. Climate,* **16,** 3599–3616.

Yeh, S.-W., and B. Kirtman, 2004: Tropical Pacific decadal variability and ENSO amplitude modulation in a CGCM. *J. Geophys. Res.,* **109,** C11009, doi:10.1029/2004JC002442.

——, J.-S. Kug, B. Dewitte, M.-H. Kwon, B. Kirtman, and F.-F. Jin, 2009: El Niño in a changing climate. *Nature,* **461,** 511–514; Corrigendum, **462,** 674.

Yu, B., and G. J. Boer, 2004: The role of the western Pacific in decadal variability. *Geophys. Res. Lett.,* **31,** L02204, doi:10.1029/2003GL01847.

Yu, J.-Y., and H.-Y. Kao, 2007: Decadal changes of ENSO persistence barrier in SST and ocean heat content indices: 1958–2001. *J. Geophys. Res.,* **112,** D13106, doi:10.1029/2006JD007654.

——, and S. T. Kim, 2011: Reversed spatial asymmetries between El Niño and La Niña and their linkage to decadal ENSO modulation in CMIP3 models. *J. Climate,* **24,** 5423–5434.

Zebiak, S. E., 1989: On the 30-60 day oscillation and the prediction of El Niño. *J. Climate,* **2,** 1381–1387.

Zhang, Y., J. M. Wallace, and D. S. Battisti, 1997: ENSO-like interdecadal variability: 1900–93. *J. Climate,* **10,** 1004–1020.